Research Paper

GEOSPHERE

GEOSPHERE; v. 13, no. 3

doi:10.1130/GES01439.1

10 figures; 1 table

CORRESPONDENCE: bdrenth@usgs.gov

CITATION: Drenth, B.J., Grauch, V.J.S., Ruleman, C.A., and Schenk, J.A., 2017, Geophysical expression of buried range-front embayment structure: Great Sand Dunes National Park, Rio Grande rift, Colorado: Geosphere, v. 13, no. 3, p. 974–990, doi:10.1130/GES01439.1.

Received 6 October 2016
Revision received 27 February 2017
Accepted 7 April 2017
Published online 10 May 2017

GOLD OPEN ACCESS

THE GEOLOGICAL SOCIETY OF AMERICA®

Geophysical expression of buried range-front embayment structure: Great Sand Dunes National Park, Rio Grande rift, Colorado

Benjamin J. Drenth[1], V.J.S. Grauch[1], Chester A. Ruleman[2], and Judith A. Schenk[3]

[1]U.S. Geological Survey, Crustal Geophysics and Geochemistry Science Center, PO Box 25046, MS 964, Denver, Colorado 80225, USA
[2]U.S. Geological Survey, Geology and Environmental Change Science Center, PO Box 25046, MS 980, Denver, Colorado 80225, USA
[3]Colorado School of Mines, 1500 Illinois St., Golden, Colorado 80401, USA

ABSTRACT

Great Sand Dunes National Park and Preserve (GRSA, Colorado) lies along the eastern margin of the San Luis Basin and the tectonically active Sangre de Cristo fault system that are part of the northern Rio Grande rift. GRSA lies within a prominent embayment in the range front where two separate sections of the Sangre de Cristo fault system intersect. Fault scarps are observed along both intersecting fault zones within older basin-fill alluvium, but have been obscured by the actively migrating dunefield. The dune sand is also strongly magnetic, locally limiting the usefulness of aeromagnetic methods for mapping concealed structure. This study uses airborne geophysical methods, primarily airborne gravity gradient data, along with constraints from geologic mapping and limited subsurface data and groundwater modeling, to interpret the subsurface basin geometry and range-front structure of the embayment. Using forward modeling of the gravity gradient data and locations of faults inferred from gravity gradient and aeromagnetic lineaments, several previously unrecognized tectonic elements are interpreted adjacent to the range front. Some of the largest rift-related fault offsets are demonstrated to be basinward of the normal fault zones mapped at the surface along the range front of the Sangre de Cristo Mountains, along faults concealed under the dunefield and subparallel to the two fault sections. A fault-bounded structural bench, likely composed of Proterozoic rocks, underlies most of the high dunefield at depths of 500 m to 1 km. The bench is truncated on its southwest margin by a northwest-trending, southwest-dipping normal fault. A northeast-trending, northwest-dipping normal fault with ~600 m of estimated relief lies under the southern margin of the dunefield and bounds a structurally higher bench of Proterozoic rocks concealed at <400 m depth near the range front. The northwest- and northeast-trending geophysical lineaments generally correspond well with the trends of faults mapped at the surface, and with both pre- and syn-rift structures in the Sangre de Cristo Mountains. Aeromagnetic anomalies are explained by variations in the magnetization of pre-rift rocks, and the strongly magnetic dune sand.

INTRODUCTION

Geophysical methods are critical for mapping rift basin structure and active faults, particularly in regions where depositional rates across active faults are in equilibrium with or exceed tectonic displacement rates, thus concealing the recognition of sections of faults. Due to paleoseismic events and young sedimentary cover that conceals significant parts of the fault zones, surficial fault traces are discontinuous or terminate at active surficial process boundaries such as dune margins and creeks. The concealed extents of discontinuous fault traces have been mapped successfully using high-resolution aeromagnetic surveys in several areas of the Rio Grande rift (Grauch and Drenth, 2009; Grauch and Ruleman, 2013), but interpretation of such surveys is hindered where topographic features composed of magnetic sediments, such as sand dunes, cause interference (Grauch and Hudson, 2007).

The study area is largely coincident with Great Sand Dunes National Park and Preserve (abbreviated by National Park Service as GRSA) in south-central Colorado. GRSA lies along the eastern margin of the San Luis Basin, one of the northernmost major basins that compose the Rio Grande rift (Fig. 1). The present-day basin can be crudely regarded as an east-tilted half-graben, with the precipitous Sangre de Cristo Mountains range front and the tectonically active, west-dipping Sangre de Cristo fault system marking its eastern side. Complex interactions between adjacent fault zones have created prominent embayments and salients in the range front, and GRSA lies within a prominent embayment where separate sections of the Sangre de Cristo fault system intersect.

The subsurface basin geometry and associated structure within the embayment are poorly understood because: (1) the active dunefield and alluvial processes on adjacent steep piedmonts rapidly remove or conceal underlying strata, structures, and traces of paleoseismic surface ruptures from direct observation; (2) the topographically rugged dunes inhibit land access for ground geophysical measurements and drilling; and (3) the dune sand is strongly magnetic, meaning that the aeromagnetic signature of buried faults and related structures is ambiguous due to interference of magnetic anomalies produced by the sand. These challenges necessitate the use of multiple airborne

Figure 1. Physiography and geography of the San Luis Basin, Colorado and New Mexico. Red box shows the area of Figure 2. Sangre de Cristo fault system is shown as a heavy black line. Inset map shows the location of the figure in relation to the Rio Grande rift. N.P.—National Park.

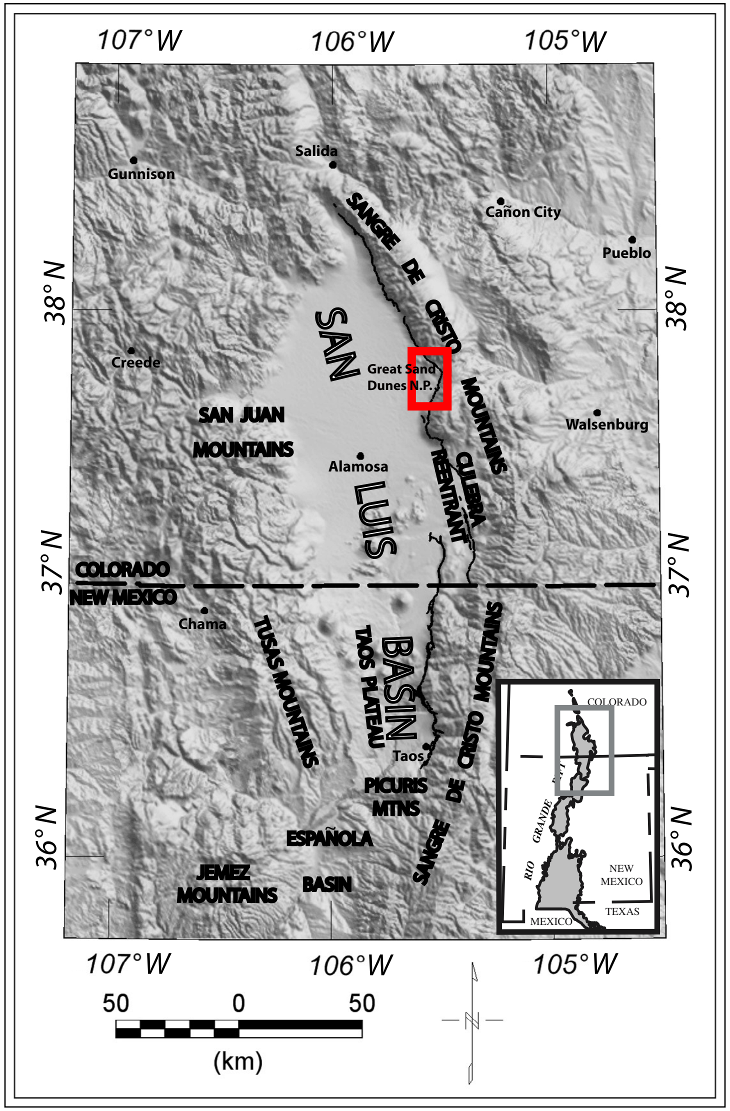

geophysical methods, particularly gravity methods, to study the local basin margin geometry, subsurface structure, and potential significance for seismic hazards. This study uses aeromagnetic and airborne gravity gradient (AGG) geophysical data, along with constraints from geologic mapping, limited subsurface data, and groundwater modeling, to interpret the subsurface basin geometry and range-front structure of the embayment. AGG data in particular are rare and give an unusually detailed view of subsurface structure. To our knowledge, this study presents the only detailed geologic interpretation of AGG data in such an environment. An airborne electromagnetic survey was flown nearby for different purposes (Ball et al., 2015), but it overlaps only a small portion of our study area and has limited depth penetration (<300 m).

GEOLOGIC BACKGROUND

The Sangre de Cristo fault system bounds the east side of the San Luis Basin, part of the 25–30 Ma to present Rio Grande rift (Hudson and Grauch, 2013). The fault system separates topographically high pre-rift rocks of the Sangre de Cristo Mountains on the east from rift basin–related sediments on the west (Fig. 2). At GRSA, a large dunefield is situated at the range front within the embayment.

The Sangre de Cristo Mountains in the study area are predominantly comprised of Paleo- and Mesoproterozoic igneous and metamorphic rocks deformed and altered through multiple tectonic and magmatic episodes (Lindsey et al., 1983, 2012; Johnson et al., 1987, 1989; Bruce and Johnson, 1991; Kellogg, 1999; Jones and Connelly, 2006; Lindsey, 2010). The Proterozoic geology is dominated by intermediate- and felsic-composition plutonic rocks in the areas of geophysical coverage (units Xii and Xif, Fig. 2). Locally, the Proterozoic rocks are unconformably overlain by clastic sedimentary rocks of the Pennsylvanian Minturn Formation, shed off the Ancestral Rockies (Kluth, 1986; Lindsey et al., 1986) and transported eastward along a series of Laramide reverse, thrust, and lateral ramp faults (ca. 70–50 Ma; Tweto, 1975). A Laramide highland likely resulted from this tectonic event and occupied the general geographic area that is now the range front during Late Cretaceous time (e.g., Sales, 1983). Granitic stocks and plutons, some as young as Oligocene, locally intrude the Proterozoic and Pennsylvanian rocks (Johnson et al., 1987; Johnson and Bruce, 1991). Proterozoic mafic plutons are also present nearby, but none have been identified within the study area.

Syn-rift sediments that accumulated within subsiding basins of the Rio Grande rift are classified as the Santa Fe Group (Spiegel and Baldwin, 1963; Ingersoll et al., 1990; Brister and Gries, 1994; Chapin and Cather, 1994; Ruleman et al., 2013). In the northern San Luis Basin, Santa Fe Group sediments were deposited on Oligocene volcanic and volcaniclastic rocks. The Santa Fe Group post-dates the youngest ash-flow tuffs (<ca. 28 Ma) erupted from the San Juan volcanic field (largely coincident with the San Juan Mountains, Fig. 1) and is as young as Middle Pleistocene age (Ingersoll et al., 1990; Brister and Gries, 1994; Connell et al., 1999; Thompson et al., 2015). The ash-flow tuffs are known to exist under significant portions of the San Luis Basin in a package that thins away from the San Juan Mountains (Brister, 1990; Brister and Gries, 1994).

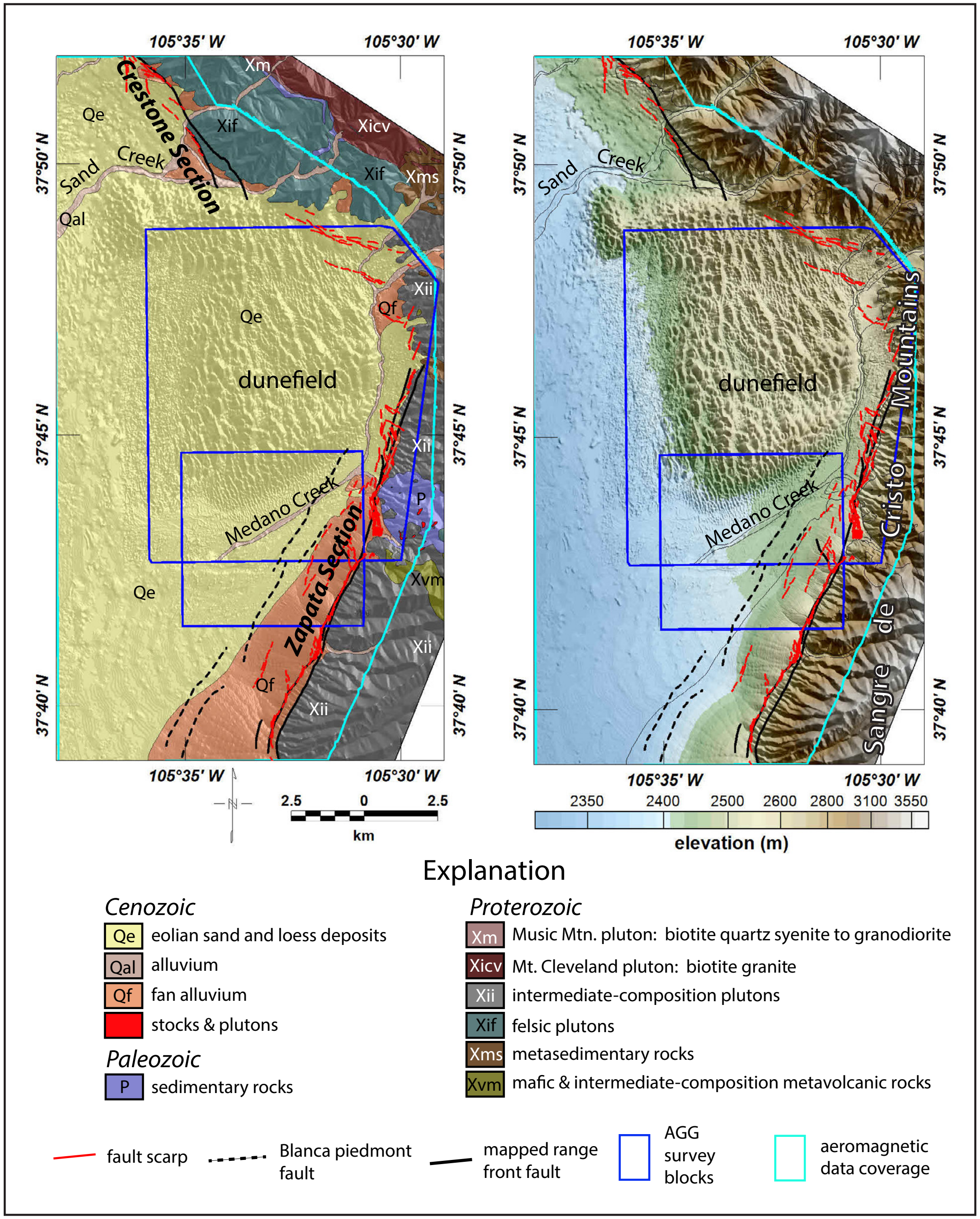

Figure 2. Geology (Lindsey et al., 1983, 2012; Johnson et al., 1987, 1989; Bruce and Johnson, 1991; Jones and Connelly, 2006; Lindsey, 2010; Grauch et al., 2013; T. Klein, 2014, personal commun.) and physiography of the study area, with boundaries of geophysical surveys (blue boxes and light blue polygon). Thrust faults in the Sangre de Cristo Mountains are not shown. Fault scarps are from unpublished mapping by C.A. Ruleman. AGG—airborne gravity gradient.

None crop out in the range front near the study area. Locally, the dominant shallow constituent of the Santa Fe Group is the Alamosa Formation (Siebenthal, 1910), composed mainly of thin beds of gravel, sand, silt, and clay that are poorly to moderately consolidated (Brister and Gries, 1994; Madole et al., 2008, 2013).

Quaternary deposits at GRSA include several ages of fan alluvium and volumetrically minor glacial deposits near the range front, but are dominated at the surface by eolian deposits that include sabkha and sand sheet deposits and culminate in a 78 km^2 dunefield (Valdez et al., 2007; Madole et al., 2008, 2013). Individual dunes reach several kilometers long and are tens to hundreds of meters high. Shallow drill holes around the periphery of the dunes suggest that eolian sand is only several meters thick and overlies several meters of alluvial fan and piedmont sediment (Madole et al., 2008, 2013). The dune sand is unusually strongly magnetized for unconsolidated sediments (Grauch et al., 2013).

A borehole-constrained interpretation of seismic reflection data indicates a ~6.4 km thickness of Santa Fe Group (Kluth and Schaftenaar, 1994) only ~10 km west of the dunefield (Baca graben of Gaca and Karig, 1966), demonstrating the profound significance of buried elements of the Sangre de Cristo fault system to basin geometry. The structural origin of the embayment is not well understood, although it is suspected to be related to asperities in pre-rift thrust fault systems (e.g., lateral ramps) that controlled development of the rift-related normal fault system (Kellogg, 1999; Ruleman and Machette, 2007). An empirical relationship exists between the modern rift-bounding fault system and preexisting structures formed during the Laramide orogeny (Kellogg, 1999; Wallace, 2004) and possibly earlier tectonic episodes. The surficial trace of active faulting is commonly along trend with, truncated by, projected into, or discontinuously shifted proximal to intersections with projections of preexisting faults exposed within the footwall bedrock.

Within the study area, the Sangre de Cristo fault system is broken into two generally steeply west-dipping normal fault zone sections that intersect at the dunefield: the northwest-trending Crestone section to the north, and the north-northeast–trending Zapata section to the south (Ruleman and Machette, 2007; Kirkham, 2012a, 2012b). The angle between the two segments approaches 90° at GRSA, forming the physiographic and structural embayment (Figs. 1 and 2) in the range front. Surface ruptures preserved along the Crestone section trend northwest subparallel to the mountain front and to Laramide thrusts exposed in the adjacent Sangre de Cristo Mountains. Rectilinear jogs in the mountain front occur locally where the range-bounding fault zone intersects older structures in the adjacent footwall bedrock. Along the Zapata section, footwall structure is much more complex (Johnson et al., 1987) and active faulting has occurred on northeast-trending faults. Several short, northwest-trending lineaments (extending across the dunefield from the Crestone section?) are preserved along the Zapata section as probable relict, Middle Pleistocene surface ruptures. These northwest-trending lineaments, interpreted as a fault zone, are cross cut by Late Pleistocene to Holocene displacements on northeast-trending faults (C.A. Ruleman, unpublished mapping, 2006–2015).

Aeromagnetic data elsewhere along the range front provide evidence for significant fault offsets along concealed structures located basinward of the range-front fault zones. Along the Crestone section north of the study area, aeromagnetic lineaments are interpreted to reflect a down-to-the-southwest normal fault zone subparallel in trend to the range-bounding fault zone, but located ~5 km to the southwest (Grauch et al., 2012; Grauch and Ruleman, 2013). South of the study area, the Blanca piedmont fault zone is generally along the range front and interpreted as a set of synthetic, subparallel normal faults located 2–3 km west of the range-front fault zone (Grauch et al., 2013) (Fig. 2). In each case, the areas between the range-bounding and intra-basin fault zones are interpreted to contain benches of pre-rift rocks with gentle basinward dips buried under <1 km of sediments and locally a thin veneer of pediment gravel along the range front. In the case of the Blanca piedmont fault zone, detailed modeling of aeromagnetic and airborne electromagnetic data indicates that faulting has offset both pre-rift rocks as well as overlying sediments (Grauch et al., 2013).

GEOPHYSICAL DATA AND METHODS

Aeromagnetic Data

Aeromagnetic anomalies reflect lateral variations of total magnetization, the vector sum of induced and remanent magnetizations (e.g., Blakely, 1995; Hinze et al., 2013). Induced magnetization is proportional to magnetic susceptibility and has the same direction as the present-day ambient field (inclination 65°, declination 9° in the study area). Remanent magnetization is related to the age and nature of a rock's formation and subsequent geologic history, and may be oriented in a different direction or directions than that of the induced magnetization. Anomalies produced by intermediate- and felsic-composition plutonic rocks are typically dominated by induced magnetization (Clark, 1999), such as those exposed locally in the Sangre de Cristo Mountains. Unconsolidated sediments are normally weakly magnetized. Dune sand at GRSA is a notable exception, with magnetic susceptibilities in the range of 0.010 SI from unpublished measurements by the authors. These values are unusually high for sediments (Grauch and Hudson, 2011). The dune sand is assumed to have negligible remanent magnetization, although a small contribution from detrital remanent magnetization is possible (Hudson et al., 2008).

Total-field aeromagnetic data were acquired by a high-resolution (150 m line spacing, 100 m above the ground along north-south traverse lines with east-west tie lines) helicopter survey (Drenth et al., 2009). A reduction-to-pole (RTP) transform, a standard technique to center anomalies over their sources (Baranov and Naudy, 1964; Blakely, 1995), was applied to the aeromagnetic data using an inclination of 65° and declination of 9° (Fig. 3A). The effects of relatively shallow magnetic sources, such as the dune sand, can be emphasized by calculation of the vertical derivative of the RTP anomalies (Blakely, 1995), shown in Figure 3B. The effects of relatively deep and/or broad magnetic sources, such as buried Proterozoic rocks, can be isolated using low-pass filtering parameters determined by matched filtering (Syberg, 1972; Phillips, 2001).

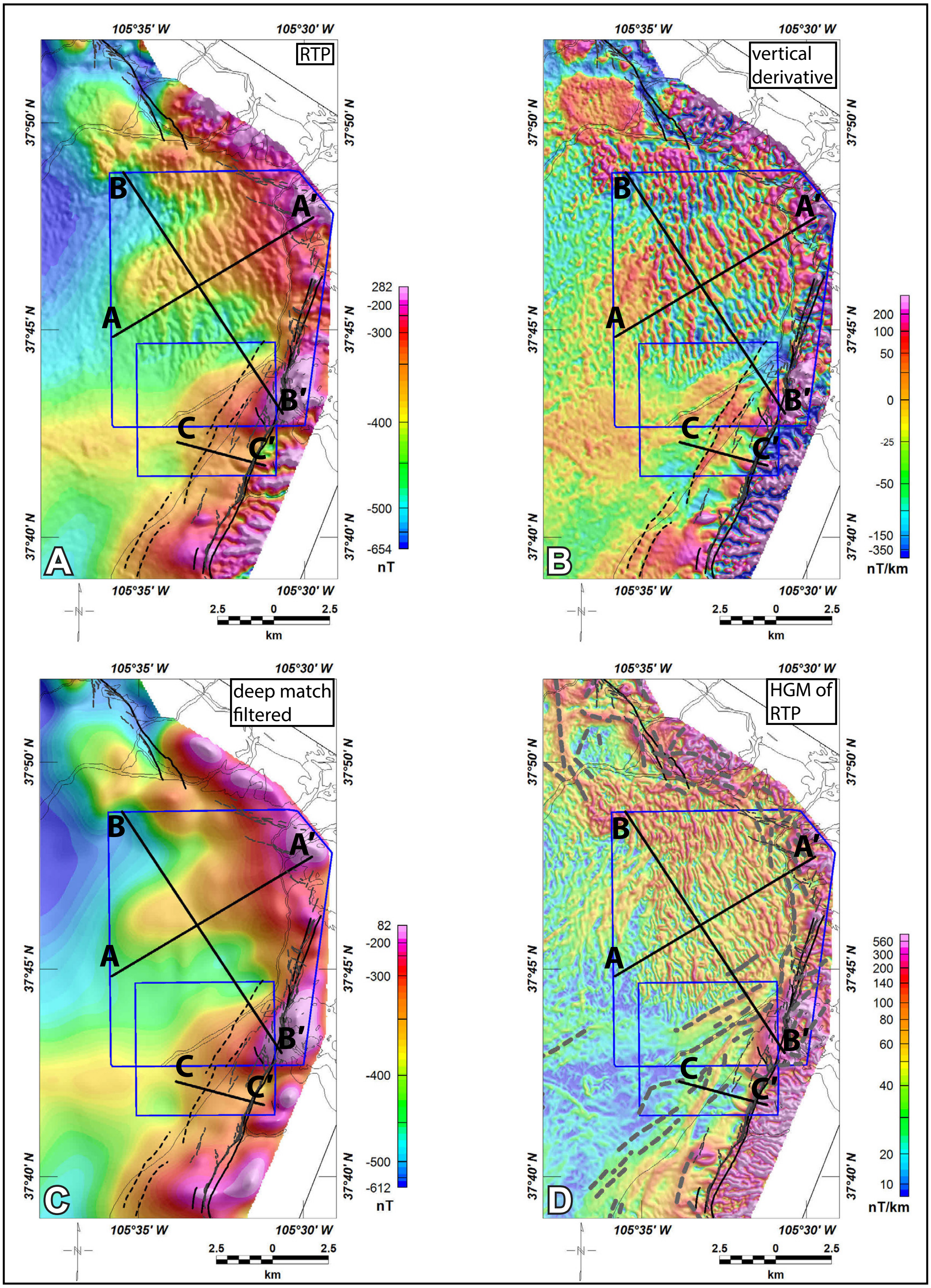

Figure 3. Aeromagnetic data. Linework including faults from Figure 2 is shown for spatial reference. Locations of profile models A-A′, B-B′, and C-C′ (Figs. 7–9) are shown. A: Reduced-to-pole (RTP) total-field magnetic anomalies. B: Vertical derivative of RTP total-field anomalies. C: Estimated effects of relatively deep and/or broad magnetic sources from matched filtering. D: Horizontal gradient magnitude (HGM) of RTP total-field anomalies. Heavy-dashed gray lines indicate new interpretations of lineaments that may be related to faulting.

Matched filtering gives a physical basis to low-pass filtering based on modeling the contribution of shallow magnetic sources in the wavenumber domain. The match filtered RTP data are shown in Figure 3C, with the short wavelengths due to shallow magnetic sources removed. Finally, magnetization contrasts may be highlighted using the horizontal gradient magnitude (HGM) of the RTP field (Cordell and Grauch, 1985; Grauch and Cordell, 1987; Grauch and Hudson, 2007). This is based on the principle that magnetic gradients reach maximum values (are steepest) over near-vertical magnetization contrasts. The HGM of the RTP field (Fig. 3D) is here used to map lineaments suspected to be related to faults, although it is possible that some lineaments mapped here are solely (i.e., unfaulted) lithologic contacts.

Airborne Gravity Gradient Data

Airborne gravity gradient (AGG) anomalies reflect lateral variations of density. Unlike traditional gravity field surveys on the ground, AGG surveys involve the measurement of the full gravity gradient tensor or portions of the full tensor from an airborne platform (e.g., Dransfield and Christensen, 2013, and references therein). Large density contrasts between low-density syn-rift sediments and older rocks make gravity and gravity gradient data useful for defining the configuration of basins within the Rio Grande rift (Cordell, 1976, 1978, 1979; Keller et al., 1984; Grauch and Keller, 2004; Grauch et al., 2006, 2009; Drenth et al., 2011, 2013b; Grauch and Connell, 2013).

For this study, a partial-tensor helicopter survey (Drenth et al., 2013a) was flown in two partially overlapping blocks (Figs. 2, 4, and 5): a northern block with 100 m line spacing at ~80 m above the ground, and a southern block with 50 m line spacing at ~40 m above the ground. Each survey block used north-south traverse lines and east-west tie lines. The full gravity gradient tensor was calculated using Fourier methods, which can generate spurious effects along the edges of the survey blocks (e.g., Drenth et al., 2013a). Data from the two blocks cannot be digitally merged in rigorous fashion, due to the differences in resolution (Kass, 2013) and the presence of edge effects.

Although the full gradient tensor was obtained from the AGG survey, only the vertical gravity gradient (Gzz) is presented here because it is the most visually and geologically intuitive. For Gzz data, positive anomalies (or highs) occur over areas of relatively high density, such as areas where sediments are thin or missing. Negative anomalies (or lows) occur over areas of relatively low density, such as areas with thick sediments. Because AGG data are the derivatives of the gravity field, AGG anomalies better reflect shallower density contrasts than do gravity anomalies, as they emphasize shorter-wavelength components of the field that are typically related to shallow sources. The AGG data were processed to remove noise inherent to gradiometer systems and measurements, as well as noise common to all types of airborne geophysical data (e.g., Dransfield and Christensen, 2013). Even after these corrections, noise arising from unpredictable variables commonly remains.

A density of 1800 kg/m^3, a value found by Nettleton profiling (Nettleton, 1942) to be appropriate for unsaturated dune sand (Drenth, 2013), was used to compute the terrain-corrected Gzz field (Figs. 4A and 5A). To reduce short-wavelength anomalies due to remaining noise, an upward continuation filter was applied to highlight anomalies of interest to this study (Figs. 4B and 5B). Upward continuation emphasizes relatively deep and/or broad features and suppresses short-wavelength noise (Blakely, 1995). A continuation distance of 200 m was subjectively determined to give the best combination of noise suppression and retention of important anomalies. The locations of density contrasts, such as those formed by contacts and faults, can be mapped using the HGM of the gravity field in a manner analogous to that described above for magnetic data (Cordell, 1979; Cordell and Grauch, 1985). The HGM of the gravity field (Figs. 4C and 5C) was calculated using horizontal tensor components (Gxz and Gyz, not shown) measured as part of the AGG survey, as opposed to being calculated in the traditional way based on differences in gravity values between neighboring grid points (e.g., Blakely and Simpson, 1986).

Geophysical Expression of Geologic Features

Aeromagnetic anomalies are dominated by the combined effects of magnetized sediments, including the dunefield (best visualized on Fig. 3B), and pre-rift rocks that crop out along the range front and extend westward under the basin (best visualized on Fig. 3C).

East of the range front into the footwall of the Sangre de Cristo fault system, aeromagnetic highs closely mimic the shape of terrain in areas of intermediate-composition plutons (unit Xii of Fig. 2), and over felsic plutons (unit Xif of Fig. 2) in the vicinity of Sand Creek, indicating significant magnetizations for those rocks. North of the Sand Creek area, anomalies are not systematically consistent with the outcrop pattern of the felsic plutons, indicating that the plutons there are weakly magnetized. The highest-amplitude aeromagnetic anomalies occur over outcrops of stocks and plutons of unknown age, both within (Figs. 2 and 3A) and south of the study area. Unlike the anomalies over other rocks in the range front, these anomalies are broader and do not mimic the shape of terrain, and source rocks are thus inferred to be largely buried. Oligocene plutons exposed in the range front south of the study area (Johnson and Bruce, 1991) are known to be strongly magnetized, based on aeromagnetic data not shown here (Drenth et al., 2009). Other possible sources for the magnetic anomalies are Proterozoic mafic intrusive rocks. Anomalies with similar shapes and amplitudes are here interpreted (see next paragraph) to reflect other strongly magnetized rocks, thought to be plutons, that in most cases are not exposed at the surface.

The interpreted pattern of variably magnetized Proterozoic rocks and strongly magnetized plutons was extended westward under the basin by interpretation of the match filtered aeromagnetic anomalies (Fig. 6). Boundaries between pre-rift crystalline rocks with different magnetizations were located by calculating the HGM of the matched filtered anomalies (not shown) and connecting the different magnetization zones with outcrops at the range front as appropriate.

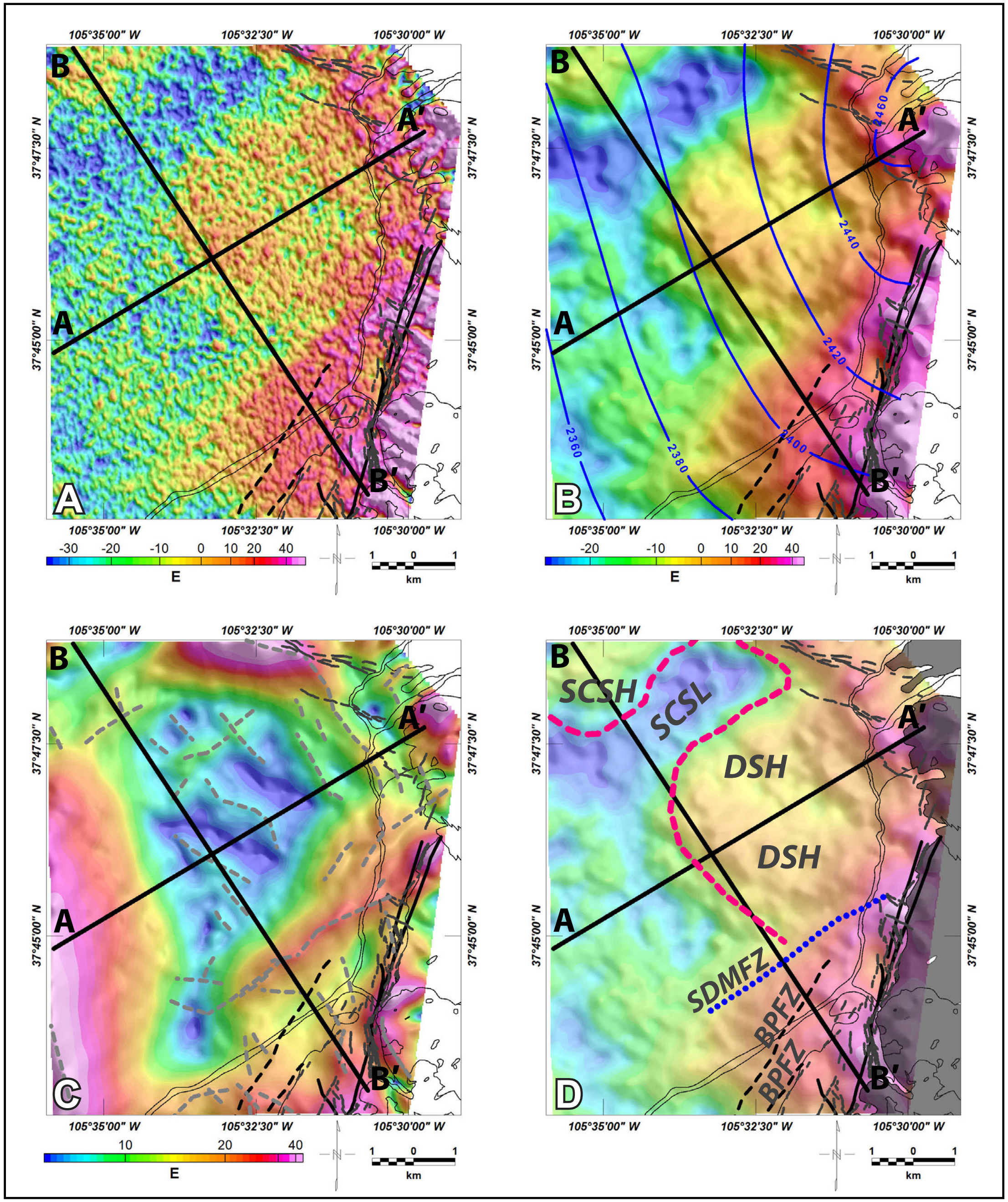

Figure 4. Airborne gravity gradient data for the northern block (see Fig. 2 for location). E—Eötvös. Linework from Figure 2 is shown for spatial reference. Locations of profile models A-A′ and B-B′ (Figs. 7–8) are shown. A: Gzz (vertical gravity gradient) data, terrain corrected using a density of 1800 kg/m³. B: Gzz data from A, upward continued 200 m. Blue contours represent average December water table elevations (HRS Water Consultants, 2007) (contour interval 20 m). C: Horizontal gradient magnitude of the gravity field. Heavy-dashed gray lines indicate new interpretations of lineaments that may be related to faulting (some lineaments are better expressed in Fig. 5C). D: Selected tectonic features discussed in the text. Grayed area is bedrock of the range front. Background colors are upward-continued Gzz data (from B). DHS—dunefield structural high; SCSH—Sand Creek structural high; SCSL—Sand Creek structural low; BPFZ—Blanca piedmont fault zone; SDMFZ—south dunefield margin fault zone.

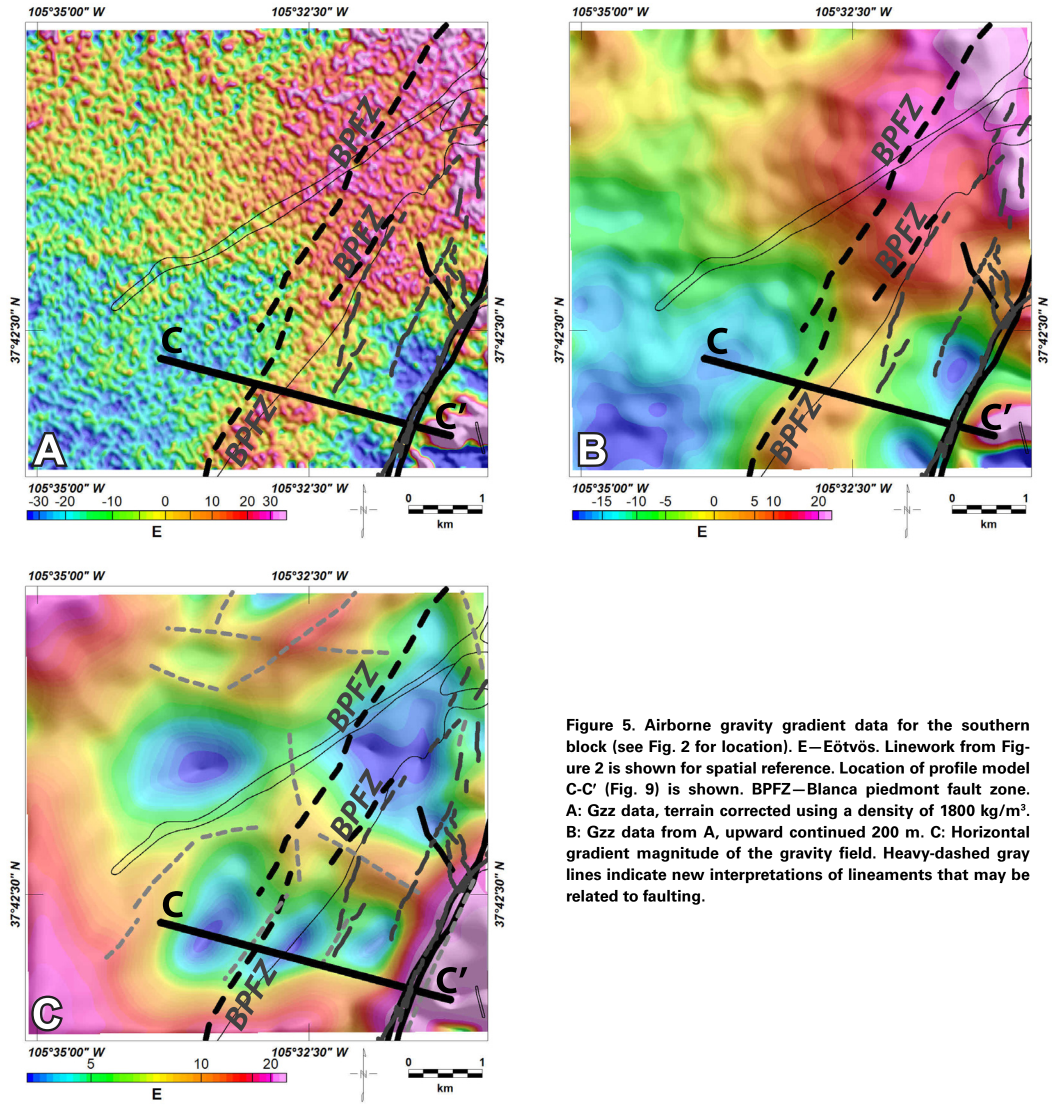

Figure 5. Airborne gravity gradient data for the southern block (see Fig. 2 for location). E—Eötvös. Linework from Figure 2 is shown for spatial reference. Location of profile model C-C′ (Fig. 9) is shown. BPFZ—Blanca piedmont fault zone. A: Gzz data, terrain corrected using a density of 1800 kg/m³. B: Gzz data from A, upward continued 200 m. C: Horizontal gradient magnitude of the gravity field. Heavy-dashed gray lines indicate new interpretations of lineaments that may be related to faulting.

The resulting interpretation is only semiquantitative, and estimates of absolute magnetic susceptibilities assigned to the different zones are geologically reasonable but quantitatively arbitrary (discussed further below). Rocks assigned to the zone of weakest magnetizations are represented in outcrop by unit Xif north of Sand Creek (Fig. 2). Units Xii and Xif in the vicinity of Sand Creek are representative of somewhat more strongly magnetized rocks. Areas of the most strongly magnetized pre-rift rocks are thought to represent Oligocene or Proterozoic plutons, the two ages of recognized plutons in the study area, although other unrecognized strongly magnetized rocks could produce similar anomalies and may be present.

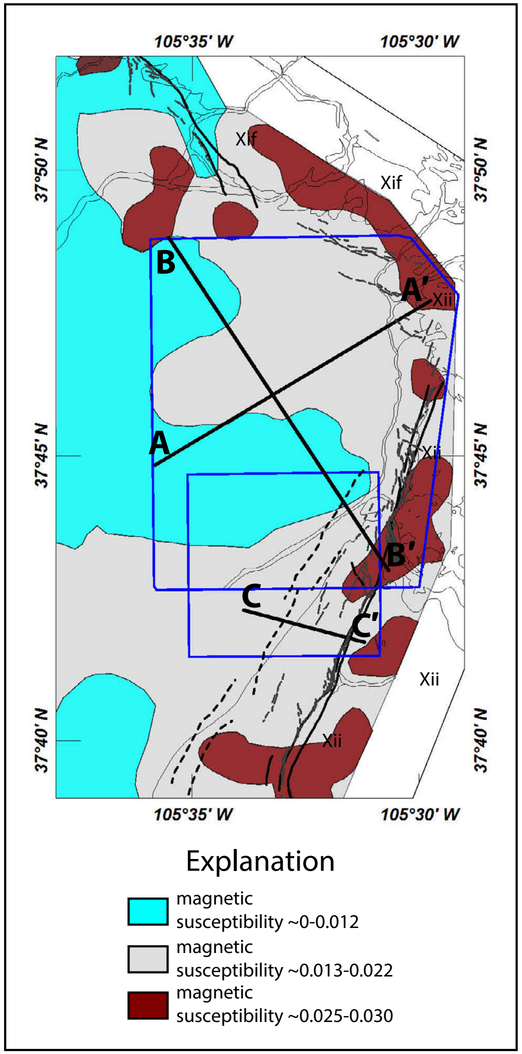

Figure 6. Semiquantitative interpretation of magnetization zones within pre-rift crystalline rocks, based upon matched filtered magnetic data (Fig. 3C) and forward profile modeling (Figs. 7–9). Linework from Figure 2 is shown for spatial reference. Locations of profile models A-A′, B-B′, and C-C′ (Figs. 7–9) are shown.

Previously interpreted and suspected faults are generally well represented in the aeromagnetic anomalies away from the dunefield (Grauch et al., 2010, 2012, 2013). The signatures of concealed faults in the dunefield are ambiguous due to the presence of strongly magnetized eolian sand that dominates the aeromagnetic signature. The geophysical expression of the mapped Sangre de Cristo range-front fault system appears as a profound break in aeromagnetic patterns, between a pattern of relatively large-amplitude short-wavelength anomalies over outcropping pre-rift rocks on the east and an area of broader and more subdued anomalies over sediments on the west (Figs. 3A and 3B; Grauch et al., 2013). Previously interpreted and suspected faults west of the range front are effectively mapped as lineaments of the HGM of the aeromagnetic anomalies (Fig. 3D; Grauch et al., 2010, 2012, 2013). Individual fault scarps are generally correlated with aeromagnetic anomalies and lineaments.

Additional interpretations of suspected faults in this study (dashed gray lines, Fig. 3D) are largely parallel to the range front. Several are interpreted to lie subparallel to the Blanca piedmont fault, suggesting that the latter is a component of a broader fault system. Others are interpreted in the Sand Creek area subparallel to and 2–3 km west of the mapped range-front fault zone (Crestone section).

The terrain-corrected and upward-continued Gzz anomalies (Figs. 4B and 5B) are interpreted to reflect variations in the thickness of sedimentary cover over pre-rift crystalline rocks, given the large density contrast between the two (e.g., Table 1). Generally values of the Gzz field get smaller to the west as the basin floor deepens. A primary feature of interest for this study is the Gzz high imaged over the dunefield (Figs. 4B and 4D), interpreted to reflect a concealed structural high (DSH on Fig. 4D) (Drenth, 2013). Another presumed structural high is imaged in the vicinity of Sand Creek, northwest of a structural low between the two highs (SCSH on Fig. 4D). The position of the Sand Creek structural high is at the edge of the AGG survey area and is incompletely imaged, meaning that its effects may not be accurately represented.

Lineaments in the AGG data are interpreted in a similar fashion as those in the aeromagnetic data. Suspected faults trending northwest and northeast are interpreted to bound the dunefield structural high (Fig. 4C). A northeast-trending fault is interpreted to lie ~2 km north of Medano Creek, near a similarly trending aeromagnetic lineament (Fig. 3D). This interpreted structure is near the southern margin of the dunefield (SDMFZ on Fig. 4D) and forms the northwest boundary of another apparent structural high that continues eastward to the range front (Figs. 4B and 4C). Terrain features with a similar northeast trend are present in this area but are likely not the sources of the geophysical lineaments because (1) the AGG data have been corrected for the effect of terrain, (2) the AGG and aeromagnetic lineaments do not strictly follow terrain trends in detail, and (3) forward modeling indicates that the AGG lineament corresponds to a major structure (see below).

The Blanca piedmont fault zone is well expressed in Gzz data in the southern part of the southern AGG survey block, where it bounds the western part of a Gzz high (Fig. 5B) and lies along a prominent gravity lineament (Fig. 5C). Another suspected, subparallel fault zone lies ~2 km to the west. However, in the northern part of the southern AGG survey block, the Blanca piedmont fault zone does not correlate well with Gzz anomalies (Figs. 5B and 5C), suggesting that it does not produce large offset of pre-rift rocks in this area. It is hypothesized that the southern dunefield margin fault becomes more important for accommodating offset of pre-rift rocks in this vicinity than the Blanca piedmont fault zone. Another possibility is that the southern dunefield margin fault locally formed earlier in the development of the Sangre de Cristo fault system than did the Blanca piedmont fault zone. This conjecture is based on the greater amount of offset on the former.

TABLE 1. GEOPHYSICAL PROPERTIES OF GEOLOGIC UNITS IN STUDY AREA, GREAT SAND DUNES NATIONAL PARK, COLORADO

Unit	Density (kg/m^3)	Density reference	Magnetic susceptibility (SI units)	Susceptibility reference
Dune sand, unsaturated	1800	Nettleton profiling, Drenth (2013)	0.004–0.006	Profile modeling, this study (not shown)
Dune sand, saturated	2080	Density log, Grauch et al. (2015)	0.004–0.006	Profile modeling, this study (not shown)
Santa Fe Group, upper 1.25 km	2170	Density logs, Grauch and Connell (2013)	0.0005	Assumed, Grauch et al. (2013)
Santa Fe Group, 1.25–2.75 km depth	2350	Density logs, Grauch and Connell (2013)	0.0005	Assumed, Grauch et al. (2013)
Strongly magnetized pre-rift rocks (Oligocene or Proterozoic plutons?)	2700	Assumed (no measurements)	0.025–0.030	Modeled, this study
Minturn Formation	2600	Assumed, Jenkins (1989)	0	Assumed small
Felsic- and intermediate-composition Proterozoic intrusions	2700	Nettleton profiling, Drenth (2013)	0–0.022	Modeled, this study

The interpretation of other AGG lineaments is more speculative. A north-northwest–trending lineament lies along the extreme southwestern margin of the northern AGG survey block and may reflect a buried fault (Fig. 4C), but problems with the data at the edge of the survey may interfere with its expression. Lineaments that trend roughly perpendicular to the range front are mapped in the southern AGG survey block (Fig. 5C) and along the southern margin of the Sand Creek structural high (Fig. 4C). These may reflect structures related to complexities in rifting or earlier structural history. As with the aeromagnetic data, individual fault scarps are generally correlated with AGG anomalies and lineaments.

FORWARD MODELING

The geologic concepts developed above were tested and refined along three forward, two-dimensional profile models (Figs. 7–9). The constraints, physical properties, and assumptions used to construct the models are discussed here. Physical properties used in the modeling are summarized in Table 1.

Modeled pre-rift rock units include Proterozoic intermediate- and felsic-composition plutonic rocks and strongly magnetized rocks thought to be Oligocene or Proterozoic plutons. The forward models were constructed using zones of different magnetizations for these crystalline rocks that are spatially consistent with the map-based interpretation of magnetization zones described above (Fig. 6). The base of these zones was arbitrarily set at 1 km below sea level for the weakly and moderately magnetized rocks in the forward models, and their susceptibilities were adjusted as needed to match the longer-wavelength portions of the magnetic anomalies. No rigorous physical property measurements are available for the strongly magnetized plutons, and they were simply modeled with higher susceptibilities thought to be reasonable for such lithologies. The shapes of the plutons are not constrained in the modeling. This is especially true of the geometries of their bottoms, and no geologic implications should be read into the shapes and locations of the bottom contacts or their relationship to the range front fault. The magnetic susceptibilities assigned to the Proterozoic rocks and inferred plutons are only semiquantitative and may not be a good approximation of true susceptibilities. The Proterozoic rocks have an estimated density of 2700 kg/m^3 based on Nettleton profiling (Drenth, 2013), and this density is used for the Proterozoic rocks in all models. The same density is applied to the inferred strongly magnetized plutons.

Minturn Formation sedimentary rocks are exposed in the range front along thrust faults (Fig. 2) and could plausibly be preserved under the basin. However, if present, it is assumed that they would be virtually indistinguishable from Proterozoic rocks in the modeling because they are thought to be weakly magnetized and have densities (2600 kg/m^3; Jenkins, 1989) similar to that of the surrounding Proterozoic rocks (2700 kg/m^3). Oligocene ash-flow tuffs also underlie parts of the San Luis Basin, but they are not exposed in the nearby range front. If present in the subsurface, they are expected to have densities (~2200 kg/m^3; Popenoe and Steven, 1969; Grauch and Hudson, 1987; R. Gries, 2007, written commun.) similar to those of the Santa Fe Group (2170–2350 kg/m^3) and thus would be indistinguishable from the syn-rift sediments in the modeling. The models assume that the Santa Fe Group and younger sediments rest directly on Proterozoic rocks, the relationship observed along the range front in and near the study area.

Density logs from the Albuquerque Basin in the central Rio Grande rift are the basis for the densities (2170–2350 kg/m^3) assigned to the Santa Fe Group (Grauch and Connell, 2013). The variable densities take compaction with increasing depth into account and have no additional stratigraphic significance. These values are assumed to be valid for all basins of the central and northern Rio Grande rift. Little is known about the magnetic susceptibilities of these sediments in this area, but they are not known to locally produce significant anomalies and are assumed to be weakly magnetized for the purposes of the modeling. The Santa Fe Group constitutes the shallowest units in the models away from areas with significant thicknesses of dune sand.

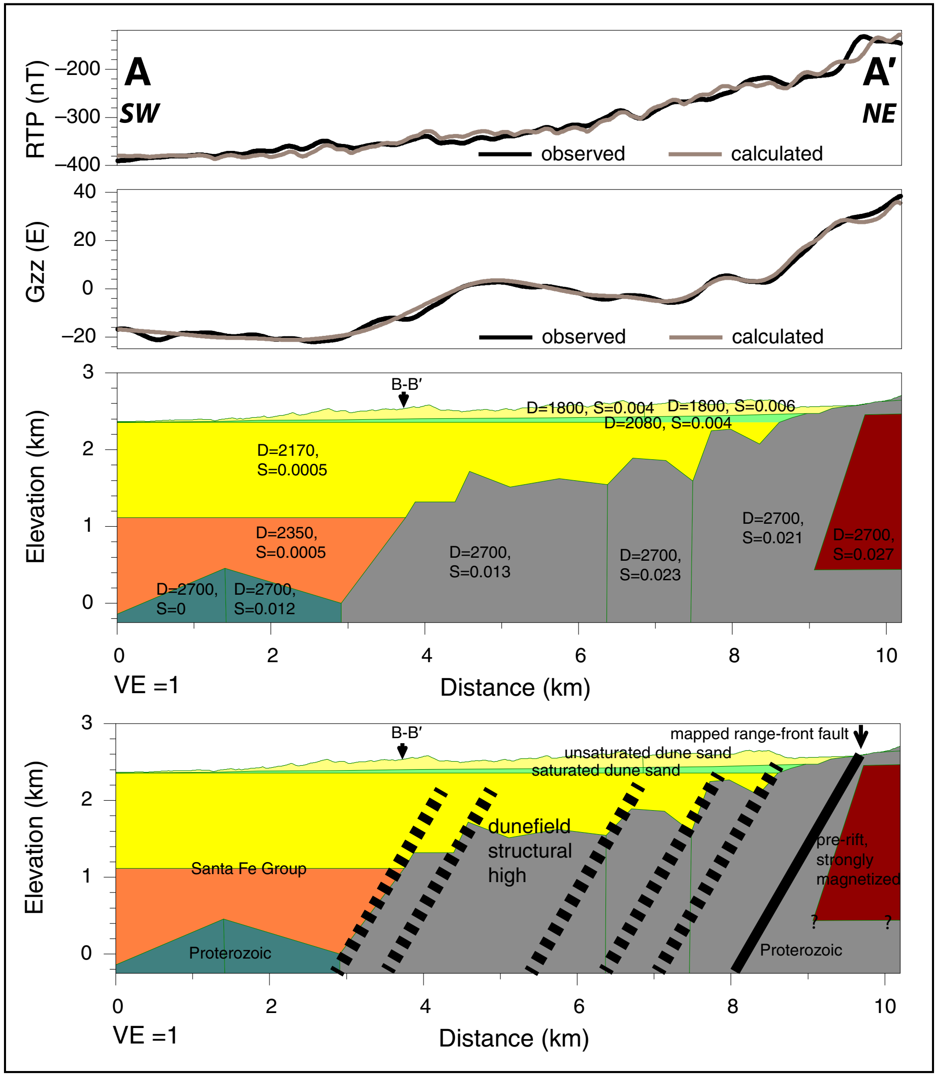

Figure 7. Geophysical profiles and forward model along A-A′ (see Fig. 3 for location). Top panel: Reduced-to-pole (RTP) aeromagnetic anomalies (Fig. 3A) and calculated model response. Second panel: Gzz (Fig. 4B) anomalies and calculated model response; E—Eötvös. Third panel: Magnetic susceptibility and density model. Densities (D) are in kg/m³, magnetic susceptibilities (S) in SI units. Bottom panel: Geologic concepts expressed in, and resulting from, this modeling. Dipping dashed black lines indicate positions of fault zones interpreted in this study. The geometry of the interpreted strongly magnetized rocks is arbitrary. VE—vertical exaggeration.

The dune sand's physical properties are significant for models A-A′ and B-B′ (Figs. 7 and 8). Its bulk magnetic susceptibility was estimated at 0.004–0.006 (SI units) from modeling the vertical derivative of the RTP aeromagnetic data over the dune field (modeling not shown). The density of unsaturated dune sand was estimated at 1800 kg/m^3 by Nettleton profiling (Nettleton, 1942; Drenth, 2013). The estimated density of saturated dune sand, 2080 kg/m^3, is from a shallow density log near the western portion of the dunefield (Grauch et al., 2015). This density value is only an estimate because the sand sampled by the density log may be mainly part of the Alamosa Formation and not directly representative of sand in the dunefield (Madole et al., 2008, 2013; Grauch et al., 2015). The water table surface comes from a groundwater model of the GRSA region (HRS Water Consultants, 2007) (Fig. 4B) and is based upon water well constraints outside the dunefield area, precipitation levels, and water budget assumptions appropriate for average December water levels for the years

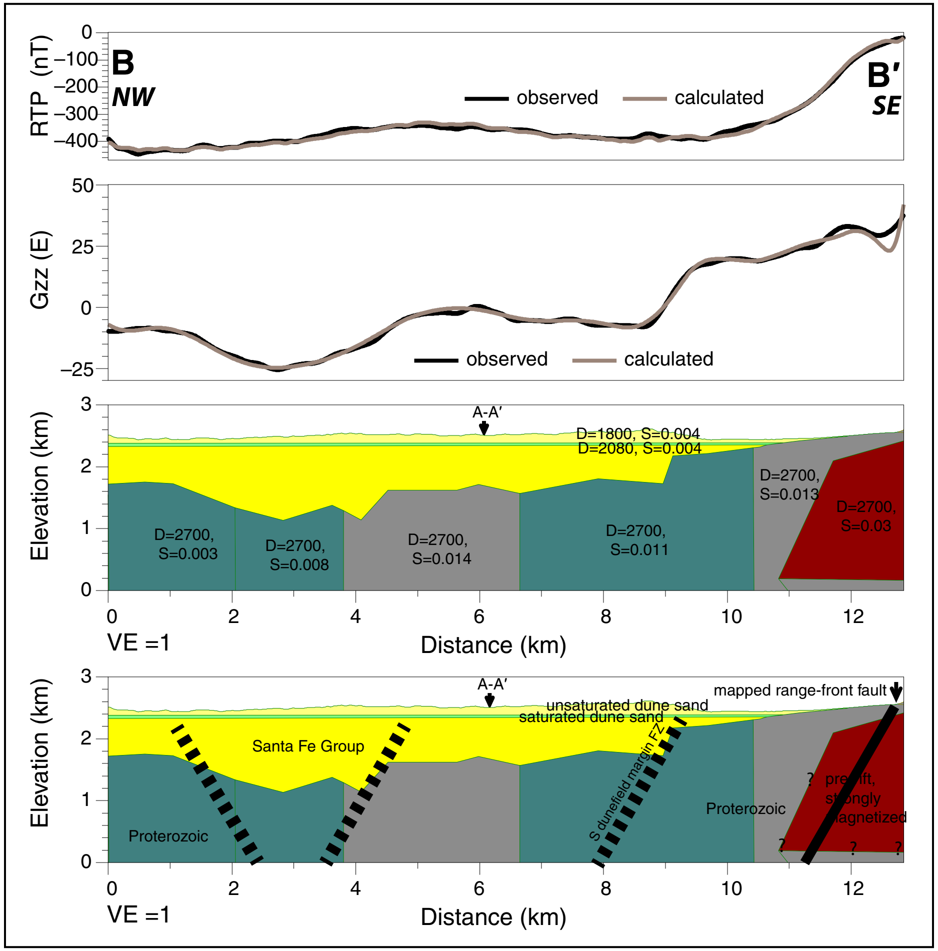

Figure 8. Geophysical profiles and forward model along B-B′ (see Fig. 3 for location). Top panel: Reduced-to-pole (RTP) aeromagnetic anomalies (Fig. 3A) and calculated model response. Second panel: Gzz (Fig. 4B) anomalies and calculated model response; E—Eötvös. Third panel: Magnetic susceptibility and density model. Densities (D) are in kg/m³, magnetic susceptibilities (S) in SI units. Bottom panel: Geologic concepts expressed in, and resulting from, this modeling. Dipping dashed black lines indicate positions of fault zones interpreted in this study. The geometry of the interpreted strongly magnetized rocks is arbitrary. VE—vertical exaggeration.

1990–2000. Average precipitation in February is approximately equal to average precipitation in December for the years 1990–2000 (data collected at station 53541 near the GRSA visitor's center). The AGG survey was flown in February, and it is assumed that the December model is appropriate.

Given the above assumptions and physical properties, the modeling proceeded by manipulating the shape of the interface between the Proterozoic rocks and Santa Fe Group until the observed Gzz data were fit. Given the large density contrast between the pre-rift rocks and younger sediments, the AGG data are thought to give the most direct representation of the basin geometry, and the magnetic data were not interpreted in the context of basin thickness. Normal faults with ~60° dips are interpreted where significant and abrupt basin thickness changes occur (Figs. 7–9). Manipulating the shape of the Proterozoic–Santa Fe Group interface could not reproduce the wavelengths and amplitudes of many of the smaller anomalies present in the AGG data, especially in areas with larger basin depths. This implies that structures, potentially faults, in the sedimentary section may be responsible for producing those anomalies.

DISCUSSION

The data and interpretations presented here, particularly those from the AGG survey, give a unique view of the structure of the extensional fault system and resulting structural and physiographic embayment. New interpreta-

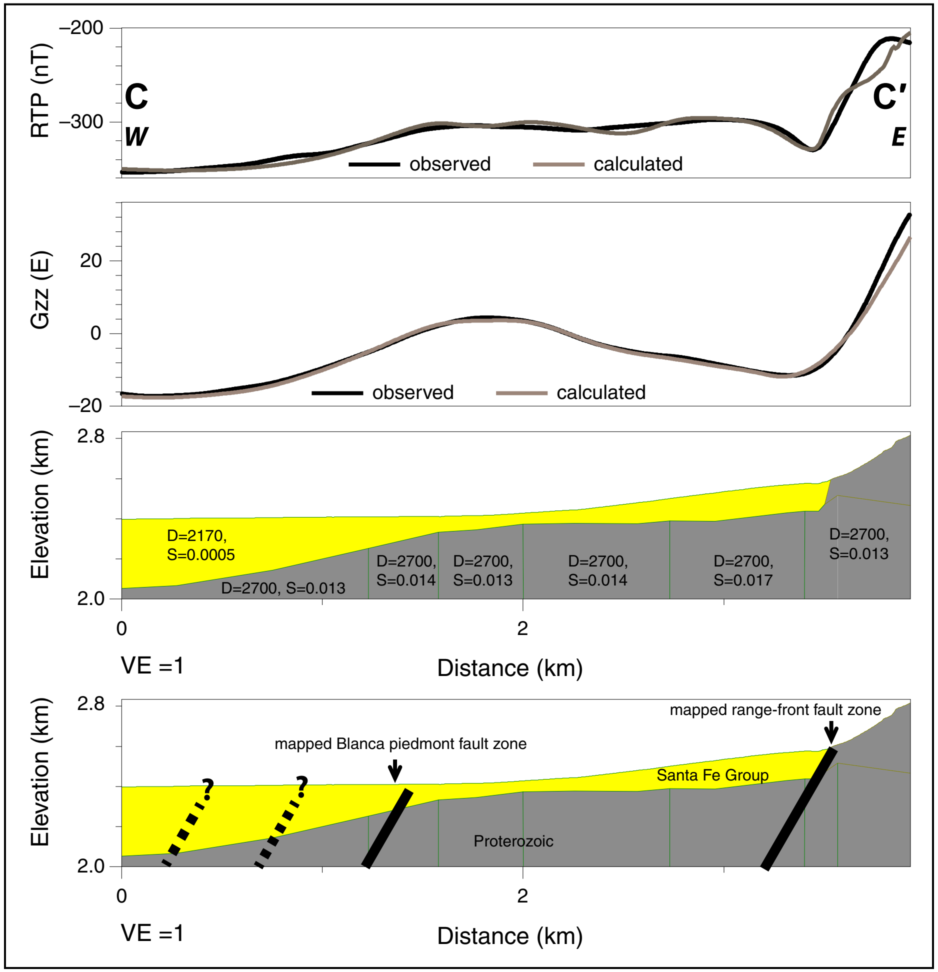

Figure 9. Geophysical profiles and forward model along C-C′ (see Fig. 3 for location). Top panel: Reduced-to-pole (RTP) aeromagnetic anomalies (Fig. 3A) and calculated model response. Second panel: Gzz (Fig. 5B) anomalies and calculated model response; E—Eötvös. Third panel: Magnetic susceptibility and density model. Densities (D) are in kg/m³, magnetic susceptibilities (S) in SI units. Bottom panel: Geologic concepts expressed in, and resulting from, this modeling. Dipping dashed black lines indicate positions of fault zones interpreted in this study, queried where less certain. VE—vertical exaggeration.

tions of the structure of the study area are presented in both qualitative (Fig. 10) and quantitative (Figs. 7–9) forms, and form the basis for the following discussion.

In each forward model, the location of the mapped range-front fault is associated with only relatively minor variations of basin thickness as compared to the larger offsets that occur along concealed basinward faults. This observation implies that the rift-related faulting observable and mapped at the surface is only a relatively small part of a largely buried fault system that controls the eastern margin of the San Luis Basin. In a broad sense, the Sangre de Cristo fault system is conceptualized as a series of westward (i.e., basinward)–down-stepping normal fault zones that bound shallowly dipping structural benches. From the geophysical data alone, it cannot be said how far the faults interpreted here extend from the top of the Proterozoic rocks upward into the sedimentary section. However, these faults are interpreted to be rift related, and as such likely extend far into the sedimentary section.

Forward modeling suggests the structural high under the dunefield is as much as 1 km deep, and the basin beyond the fault at its southwestern margin is close to 2 km deep (Figs. 7 and 10). Along the extent of A-A′, the fault at the southwestern margin of the structural high is interpreted as the dominant basin-bounding structure. The extent of the structural high is only weakly

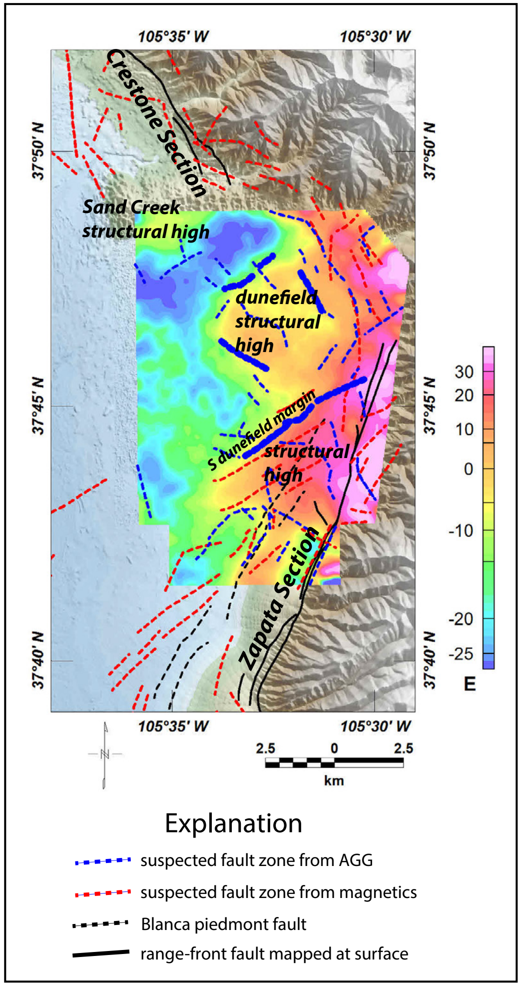

Figure 10. Summary of rift-related tectonic interpretations resulting from this study. Selected tectonic elements are labeled. Some suspected fault zones imaged from magnetics in the range front may be related to pre-rift thrust faulting. Image of upward-continued Gzz data (Figs. 4B and 5B; survey blocks crudely merged) is included as a qualitative proxy for elevation of pre-rift rocks; E—Eötvös. Heavier blue lines are interpreted concealed faults with a maximum throw of >500 m. AGG—airborne gravity gradient.

correlated with the extent of the dunefield. If the structural high has any relationship to the dunefield, it is not directly apparent. The southern dunefield margin fault zone is another major basin-bounding structure (Figs. 8 and 10). It is interpreted as a northeast-striking, down-to-the-northwest normal fault with ~600 m of vertical displacement of Proterozoic rocks (Fig. 8). This northeast-trending fault is also subparallel to nearby Medano Creek, raising the possibility of structural control on fluvial patterns and development of the local dunefield margin. However, the fault zone extends well beyond the dunefield to the southwest, so any direct relationship between structure and the extent of topographic features is not apparent.

Another shallow (<400 m deep in B-B′, Fig. 8) structural high is imaged southeast of the southern dunefield margin fault zone (labeled "structural high" on Fig. 10). It has a relatively complex shape and pattern of interpreted faulting associated with it. This structure apparently lies along the structural transition between the Blanca piedmont fault and the southern dunefield margin fault zone, and likely has a complicated history of displacement. A complex set of suspected faults with small structural offsets is interpreted in the immediate area of the structural high, possibly indicating incipient tectonic fragmentation of this structural high. South of this high area, the structural setting is relatively simple, with a shallowly buried (<150 m sedimentary cover) structural bench lying west of the range front and bounded on the west by the Blanca piedmont fault (Figs. 9 and 10).

The Sand Creek structural high (Fig. 10), incompletely imaged by AGG data, may represent shallow Proterozoic rocks bounded on the west by down-to-the-west normal faults imaged as aeromagnetic lineaments. The structural high and its western boundary lie about a kilometer south of a region of moderately high electrical resistivities (>200 ohm-m) observed from an airborne electromagnetic survey (Ball et al., 2015). The region of high resistivity, inferred as buried bedrock, is distinctly bounded on the west and south by low resistivities (20 ohm-m), inferred as sediments, which extend down to the limits of detection (200–250 m deep). These observations imply that the Sand Creek structural high, as imaged by AGG data at the north end of the survey, is part of a broader structural high that reaches shallower depths (100–200 m) to the north. It is also an area with lithologic heterogeneity within pre-rift rocks (using magnetization as a proxy for lithology; Fig. 6). Interpreted patterns of faulting are inconsistently correlated with lithologic boundaries, suggesting that the lithologic variations are independent of structure.

Faulted sediments are demonstrably a source of aeromagnetic lineaments related to the Blanca piedmont fault, in addition to faulted pre-rift rocks (Grauch et al., 2013). This study provides evidence that faulted sediments may also cause small AGG anomalies and thus may contribute to lineaments mapped as suspected faults: The fact that the geometry of the Proterozoic surface under the basin cannot entirely explain AGG anomalies, because the Proterozoic surface is too deep, implies that anomaly sources must also lie within the sedimentary section. Faulted sediments and/or sedimentary rocks are an obvious possibility. However, known density contrasts present across lithologic boundaries within the sedimentary section are small (e.g., Grauch et al., 2015), so the specific geologic origin of those density contrasts is unknown. Alternate possibilities are locally inadequate terrain corrections, and unrecognized problems with the AGG data processing.

A northeast-trending Gzz low, interpreted to reflect a structural low named the Sand Creek structural low, lies between the dunefield structural high and the Sand Creek structural high (Fig. 10). Forward modeling suggests a structure 2–3 km in width, and 300 m to 1.5 km deep relative to the surrounding pre-rift surface (Fig. 8 and other modeling, not shown). Prominent AGG lineaments lie along the north and south margins of the structure, and these are interpreted to indicate bounding faults that controlled the structure's development. These northeast trends are notably subparallel to the south dunefield margin fault zone. An alternate possibility is that the Gzz low in this area is partially or largely caused by low-density pre-rift rocks. This possibility is less likely because (1) there is no evidence for low-density pre-rift rocks in the nearby range front, and (2) the relations observed from electrical resistivity sections (discussed previously) suggest that bedrock is shallow (100–200 m) over the Sand Creek structural high but below 200–250 m depth within the Gzz low (Ball et al., 2015). The trend of the structural low, which is roughly normal to the range front, raises the possibility that it was once occupied by a prominent drainage. If so, the drainage would have formed prior to the deposition of the sediments above it (Fig. 8). Such a drainage may have contributed to the formation of what is otherwise thought to be a structural low. The Sand Creek structural low, and possible paleodrainage, is along the general northeast trend of other early to middle Cenozoic drainages in adjacent regions, and could likely be a paleodrainage that was truncated as the Sangre de Cristo fault system developed in late Cenozoic time.

Patterns of suspected faults reveal how the Zapata and Crestone sections of the Sangre de Cristo fault system project into the area of the dunefield and physiographic range front embayment. The southern dunefield margin fault zone appears to be the northernmost major structure that is more or less subparallel to the northeast-striking Zapata section and range front. North of there, northwest-trending structures subparallel to the Crestone section of the fault system are prevalent, with the exception of the interpreted faults that bound the structural low between the dunefield and Sand Creek structural highs. Given the abundance of surficial evidence for more recent offsets along northeast-trending faults, and the lack of geophysical expression of northwest-trending structures close to the range front south of the dunefield, we interpret the northeast-trending structures south of the dunefield (presumably related to the Zapata section) to locally cut the northwest-trending structures (presumably related to the Crestone section) that are prevalent under and north of the dunefield. The broad pattern suggested is Late Pleistocene migration of tectonic activity from northwest- to northeast-trending structures along the margin of the embayment.

The general regional northwest trend of the Sangre de Cristo fault system in Colorado (e.g., Figs. 1 and 2; Wallace, 2004; Ruleman and Machette, 2007), locally manifested as the Zapata section, is cross cut by a series of en echelon, northeast-trending, northwest-dipping normal faults stepping down to the <1 km depth dunefield structural high. The dunefield structural high is bound on the north by an interpreted northeast-trending graben and horst (i.e., Sand Creek structural low and structural high, respectively). The basin drops off substantially, to a thickness of ~6.4 km (Kluth and Schaftenaar, 1994), only ~10 km west of the dunefield along presumed northwest-trending structures, reflecting the dominant basin-forming structural orientation. We propose that this prominent embayment in the study area is controlled by dominant northwest-trending fault zones cut by northeast-trending fault zones.

CONCLUSIONS

Airborne geophysical data, particularly AGG data, provide a detailed and unique view of the geometry, structure, and potential seismic hazards of a prominent embayment in the Sangre de Cristo fault system at Great Sand Dunes National Park and Preserve. An entirely concealed structural high is interpreted to lie under the dunefield, and others are interpreted between the southern dunefield fault and the range front, and in the vicinity of Sand Creek. The Crestone and Zapata sections of the Sangre de Cristo fault system meet at nearly 90° in complex fashion. Some of the largest rift-related fault offsets are demonstrated to be on concealed faults subparallel to the two fault sections basinward of the range-bounding normal fault zones mapped along the Sangre de Cristo Mountains. Prominent and previously unrecognized faults interpreted from this study include a northwest-trending fault under the dunefield, and a northeast-trending fault located roughly under the southern margin of the dunefield and subparallel to Medano Creek. Northeast-trending faults are interpreted to cut northwest-trending faults within the southern half of the study area.

Aeromagnetic anomalies are interpreted to be caused by a combination of pre-rift, mainly Proterozoic rocks, and strongly magnetized sediments. The largest aeromagnetic highs are thought to be caused by Oligocene or Proterozoic mafic plutons, both known to exist in the region. The aeromagnetic expression of faulting is well developed away from the dunefield, but obscured under the dunefield by the strong magnetization of the dune sand.

ACKNOWLEDGMENTS

We thank Mark Dransfield, David Lindsey, and Mark Hudson for helpful discussions. David Lindsey, Randy Keller, Diane Doser, and Tiku Ravat provided helpful reviews. Special thanks go to GRSA staff, especially Andrew Valdez and Fred Bunch, for their enthusiastic logistical, field, and administrative support. This work was funded by the National Cooperative Geologic Mapping and Mineral Resource Programs of the U.S. Geological Survey.

REFERENCES CITED

Ball, L.B., Bloss, B.R., Bedrosian, P.A., Grauch, V.J.S., and Smith, B.D., 2015, Airborne electromagnetic and magnetic survey data of the Paradox and San Luis Valleys, Colorado: U.S. Geological Survey Open-File Report 2015-1024, 19 p., doi:10.3133/ofr20151024.

Baranov, V., and Naudy, H., 1964, Numerical calculation of the formula of reduction to the magnetic pole: Geophysics, v. 29, p. 67–79, doi:10.1190/1.1439334.

Blakely, R.J., 1995, Potential Theory in Gravity and Magnetic Applications: New York, Cambridge University Press, 441 p., doi:10.1017/CBO9780511549816.

Blakely, R.J., and Simpson, R.W., 1986, Approximating edges of source bodies from magnetic or gravity anomalies: Geophysics, v. 51, p. 1494–1498, doi:10.1190/1.1442197.

Brister, B.S., 1990, Tertiary sedimentation and tectonics: San Juan sag–San Luis Basin region, Colorado and New Mexico [Ph.D. thesis]: Socorro, New Mexico, New Mexico Institute of Mining and Technology, 267 p.

Brister, B.S., and Gries, R.R., 1994, Tertiary stratigraphy and tectonic development of the Alamosa basin (northern San Luis Basin), Rio Grande rift, south-central Colorado, *in* Keller, G.R., and Cather, S.M., eds., Basins of the Rio Grande Rift: Structure, Stratigraphy, and Tectonic Setting: Geological Society of America Special Paper 291, p. 39–58, doi:10.1130/SPE291-p39.

Bruce, R.M., and Johnson, B.R., 1991, Reconnaissance geologic map of parts of the Zapata Ranch and Mosca Pass quadrangles, Alamosa and Huerfano Counties, Colorado: U.S. Geological Survey Miscellaneous Field Studies Map MF-2168, scale 1:24,000.

Chapin, C.E., and Cather, S.M., 1994, Tectonic setting of the axial basins of the northern and central Rio Grande rift, *in* Keller, G.R., and Cather, S.M., eds., Basins of the Rio Grande Rift: Structure, Stratigraphy, and Tectonic Setting: Geological Society of America Special Paper 291, p. 5–26, doi:10.1130/SPE291-p5.

Clark, D.A., 1999, Magnetic petrology of igneous intrusions: Implications for exploration and magnetic interpretation: Exploration Geophysics, v. 30, p. 5–26, doi:10.1071/EG999005.

Connell, S.D., Koning, D.J., and Cather, S.M., 1999, Revisions to the stratigraphic nomenclature of the Santa Fe Group, northwestern Albuquerque Basin, New Mexico, *in* Pazzaglia, F.J., and Lucas, S.G., eds., Albuquerque Geology: New Mexico Geological Society 50th Annual Fall Field Conference Guidebook, p. 337–353.

Cordell, L., 1976, Aeromagnetic and gravity studies of the Rio Grande graben in New Mexico between Belen and Pilar, *in* Woodward, L.A., and Northrop, S.A., eds., Tectonics and Mineral Resources of Southwestern North America: New Mexico Geological Society Special Publication 6, p. 169–179.

Cordell, L., 1978, Regional geophysical setting of the Rio Grande rift: Geological Society of America Bulletin, v. 89, p. 1073–1090, doi:10.1130/0016-7606(1978)89<1073:RGSOTR>2.0.CO;2.

Cordell, L., 1979, Gravimetric expression of graben faulting in Santa Fe country and the Espanola basin, New Mexico, *in* Ingersoll, R.V., Woodward, L.A., and James, H.L., eds., Santa Fe Country: New Mexico Geological Society 30th Annual Fall Field Conference Guidebook, p. 59–64.

Cordell, L., and Grauch, V.J.S., 1985, Mapping basement magnetization zones from aeromagnetic data in the San Juan basin, New Mexico, *in* Hinze, W.J., ed., The Utility of Regional Gravity and Magnetic Anomaly Maps: Tulsa, Oklahoma, Society of Exploration Geophysicists, p. 181–197, doi:10.1190/1.0931830346.ch16.

Dransfield, M.H., and Christensen, A.N., 2013, Performance of airborne gravity gradiometers: The Leading Edge, v. 32, p. 908–922, doi:10.1190/tle32080908.1.

Drenth, B.J., 2013, Expression of terrain and surface geology in high-resolution helicopter-borne gravity gradient (AGG) data: Examples from Great Sand Dunes National Park, Rio Grande Rift, Colorado: The Leading Edge, v. 32, p. 924–930, doi:10.1190/tle32080924.1.

Drenth, B.J., Grauch, V.J.S., Bankey, V., and New Sense Geophysics, Ltd., 2009, Digital data from the Great Sand Dunes and Poncha Springs aeromagnetic surveys, south-central Colorado: U.S. Geological Survey Open-File Report 2009-1089, 6 p.

Drenth, B.J., Turner, K.J., Thompson, R.A., Grauch, V.J.S., Cosca, M.A., and Lee, J.P., 2011, Geophysical expression of elements of the Rio Grande rift in the northeast Tusas Mountains: Preliminary interpretations, *in* Koning, D.J., Karlstrom, K.E., Kelley, S.A., Lueth, V.W., and Aby, S.B., eds., Geology of the Tusas Mountains and Ojo Caliente: New Mexico Geological Society 62nd Annual Fall Field Conference Guidebook, p. 165–175.

Drenth, B.J., Abraham, J.D., Grauch, V.J.S., and Hodges, G., 2013a, Digital data from the Great Sand Dunes airborne gravity gradient survey, south-central Colorado: U.S. Geological Survey Open-File Report 2013-1011, 5 p.

Drenth, B.J., Grauch, V.J.S., and Rodriguez, B.D., 2013b, Geophysical constraints on Rio Grande rift structure in the central San Luis Basin, Colorado and New Mexico, *in* Hudson, M.R., and Grauch, V.J.S., eds., New Perspectives on Rio Grande Rift Basins: From Tectonics to Groundwater: Geological Society of America Special Paper 494, p. 75–99, doi:10.1130/2013.2494(04).

Gaca, J.R., and Karig, D.E., 1966, Gravity survey in the San Luis Valley area, Colorado: U.S. Geological Survey Open-File Report 66-46, 21 p.

Grauch, V.J.S., and Connell, S.D., 2013, New perspectives on the geometry of the Albuquerque Basin, Rio Grande rift, New Mexico, *in* Hudson, M.R., and Grauch, V.J.S., eds., New Perspectives on Rio Grande Rift Basins: From Tectonics to Groundwater: Geological Society of America Special Paper 494, p. 427–462, doi:10.1130/2013.2494(16).

Grauch, V.J.S., and Cordell, L., 1987, Limitations of determining density or magnetic boundaries from the horizontal gradient of gravity or pseudogravity data: Geophysics, v. 52, p. 118–121, doi:10.1190/1.1442236.

Grauch, V.J.S., and Drenth, B.J., 2009, High-resolution aeromagnetic survey to image shallow faults, Poncha Springs and vicinity, Chaffee County, Colorado: U.S. Geological Survey Open-File Report 2009-1156, 31 p.

Grauch, V.J.S., and Hudson, M.R., 1987, Summary of natural remanent magnetization, magnetic susceptibility, and density measurements from the Lake City caldera area, San Juan Mountains, Colorado: U.S. Geological Survey Open-File Report 87-182, 23 p.

Grauch, V.J.S., and Hudson, M.R., 2007, Guides to understanding the aeromagnetic expression of faults in sedimentary basins: Lessons learned from the central Rio Grande rift, New Mexico: Geosphere, v. 3, p. 596–623, doi:10.1130/GES00128.1.

Grauch, V.J.S., and Hudson, M.R., 2011, Aeromagnetic anomalies over faulted strata: The Leading Edge, v. 30, p. 1242–1252, doi:10.1190/1.3663396.

Grauch, V.J.S., and Keller, G.R., 2004, Gravity and aeromagnetic expression of tectonic and volcanic elements of the southern San Luis Basin, New Mexico and Colorado, *in* Brister, B.S., Bauer, P.W., Read, A.S., and Lueth, V.W., eds., Geology of the Taos Region: New Mexico Geological Society 55th Fall Field Conference Guidebook, p. 230–243.

Grauch, V.J.S., and Ruleman, C.A., 2013, Identifying buried segments of active faults in the northern Rio Grande rift using aeromagnetic, LiDAR, and gravity data, south-central Colorado, USA: International Journal of Geophysics, v. 2013, 804216, 26 p., doi:10.1155/2013/804216.

Grauch, V.J.S., Sawyer, D.A., Minor, S.A., Hudson, M.R., and Thompson, R.A., 2006, Gravity and aeromagnetic studies of the Santo Domingo Basin area, New Mexico, *in* Minor, S.A., ed., The Cerrillos Uplift, the La Bajada Constriction, and Hydrogeologic Framework of the Santo Domingo Basin, Rio Grande Rift, New Mexico: U.S. Geological Survey Professional Paper 1720, p. 62–86.

Grauch, V.J.S., Phillips, J.D., Koning, D.J., Johnson, P.S., and Bankey, V., 2009, Geophysical interpretations of the southern Espanola Basin, New Mexico, that contribute to understanding its hydrogeologic framework: U.S. Geological Survey Professional Paper 1761, 88 p.

Grauch, V.J.S., Fitterman, D.V., and Drenth, B.J., 2010, Finding faults using high-resolution aeromagnetic data in Great Sand Dunes National Park and vicinity, San Luis Valley, Colorado, *in* Proceedings of the 23rd SAGEEP, 2010 EEGS Annual Meeting, Keystone, Colorado, 11–15 April: EEGS/SAGEEP, p. 428–437.

Grauch, V.J.S., Drenth, B.J., Caine, J.S., Ruleman, C.A., Lindsey, D.A., and Klein, T.L., 2012, New insights into basin geometry and range-front faulting from recent geophysical surveys in northeastern San Luis Basin, Rio Grande rift, Colorado: Geological Society of America, Abstracts with Programs, v. 44, no. 6, p. 15.

Grauch, V.J.S., Bedrosian, P.A., and Drenth, B.J., 2013, Advancements in understanding the aeromagnetic expressions of basin-margin faults: An example from San Luis Basin, Colorado: The Leading Edge, v. 32, p. 882–891, doi:10.1190/tle32080882.1.

Grauch, V.J.S., Skipp, G.L., Thomas, J.V., Davis, J.K., and Benson, M.E., 2015, Sample descriptions and geophysical logs for cored well BP-3-USGS, Great Sand Dunes National Park and Preserve, Alamosa County, Colorado: U.S. Geological Survey Data Series 918, 53 p.

Hinze, W.J., von Frese, R.R.B., and Saad, A.H., 2013, Gravity and Magnetic Exploration: New York, Cambridge University Press, 512 p., doi:10.1017/CBO9780511843129.

HRS Water Consultants, 2007, Amended report, Numerical ground water model of Great Sand Dunes National Park and Preserve, 132 p.

Hudson, M.R., and Grauch, V.J.S., 2013, Introduction, *in* Hudson, M.R., and Grauch, V.J.S., eds., New Perspectives on Rio Grande Rift Basins: From Tectonics to Groundwater: Geological Society of America Special Paper 494, p. v–xii, doi:10.1130/2013.2494(00).

Hudson, M.R., Grauch, V.J.S., and Minor, S.A., 2008, Rock magnetic characterization of faulted sediments with associated magnetic anomalies in the Albuquerque Basin, Rio Grande rift, New Mexico: Geological Society of America Bulletin, v. 120, p. 641–658, doi:10.1130/B26213.1.

Ingersoll, R.V., Cavazza, W., Baldridge, W.S., and Shafiqullah, M., 1990, Cenozoic sedimentation and paleotectonics of north-central New Mexico: Implications for initiation and evolution of the Rio Grande rift: Geological Society of America Bulletin, v. 102, p. 1280–1296, doi:10.1130/0016-7606(1990)102<1280:CSAPON>2.3.CO;2.

Jenkins, R.D., 1989, An interpretation of basement structures from gravity anomalies in the central portion of the Colorado Plateau [M.S. thesis]: El Paso, University of Texas at El Paso, 174 p.

Johnson, B.R., and Bruce, R.M., 1991, Reconnaissance geologic map of parts of the Twin Peaks and Blanca Peak quadrangles, Alamosa, Costilla, and Huerfano Counties, Colorado: U.S. Geological Survey Miscellaneous Field Studies Map MF-2169, scale 1:24,000.

Johnson, B.R., Lindsey, D.A., Bruce, R.M., and Soulliere, S.J., 1987, Geologic map of the Sangre de Cristo Wilderness study area, Colorado: U.S. Geological Survey Miscellaneous Field Studies Map MF-1635-B, scale 1:62,500.

Johnson, B.R., Bruce, R.M., and Lindsey, D.A., 1989, Reconnaissance geologic map of the Medano Pass quadrangle and part of the Liberty quadrangle, Alamosa, Huerfano, and Saguache Counties, Colorado: U.S. Geological Survey Miscellaneous Field Studies Map MF-2089, scale 1:24,000.

Jones, J.V., III, and Connelly, J.N., 2006, Proterozoic tectonic evolution of the Sangre de Cristo Mountains, southern Colorado, U.S.A.: Rocky Mountain Geology, v. 41, p. 79–116, doi:10.2113/gsrocky.41.2.79.

Kass, M.A., 2013, Consequences of flight height and line spacing on airborne (helicopter) gravity gradient resolution in the Great Sand Dunes National Park and Preserve, Colorado: The Leading Edge, v. 32, p. 932–938, doi:10.1190/tle32080932.1.

Keller, G.R., Cordell, L., Davis, G.H., Peeples, W.J., and White, G., 1984, A geophysical study of the San Luis basin, *in* Baldridge, W.S., Dickerson, P.W., Riecker, R.E., and Zidek, J., eds., Rio Grande Rift: Northern New Mexico: New Mexico Geological Society 35th Fall Field Conference Guidebook, p. 51–57.

Kellogg, K.S., 1999, Neogene basins of the northern Rio Grande rift: Partitioning and asymmetry inherited from Laramide and older uplifts: Tectonophysics, v. 305, p. 141–152, doi:10.1016/S0040-1951(99)00013-X.

Kirkham, R.M., compiler, 2012a, Fault number 2321a, Northern Sangre de Cristo fault, Crestone section, *in* Quaternary Fault and Fold Database of the United States: U.S. Geological Survey, http://earthquakes.usgs.gov/hazards/qfaults (accessed October 2015).

Kirkham, R.M., compiler, 2012b, Fault number 2321b, Northern Sangre de Cristo fault, Zapata section, *in* Quaternary Fault and Fold Database of the United States: U.S. Geological Survey, http://earthquakes.usgs.gov/hazards/qfaults (accessed October 2015).

Kluth, C.F., 1986, Plate tectonics of the Ancestral Rocky Mountains, *in* Peterson, J.A., ed., Paleotectonics and Sedimentation: American Association of Petroleum Geologists Memoir 41, p. 353–369.

Kluth, C.F., and Schaftenaar, C.H., 1994, Depth and geometry of the northern Rio Grande rift in the San Luis Basin, south-central Colorado, *in* Keller, G.R., and Cather, S.M., eds., Basins of the Rio Grande Rift: Structure, Stratigraphy, and Tectonic Setting: Geological Society of America Special Paper 291, p. 27–38, doi:10.1130/SPE291-p27.

Lindsey, D.A., 2010, The geologic story of Colorado's Sangre de Cristo Range: U.S. Geological Survey Circular 1349, 14 p.

Lindsey, D.A., Johnson, B.J., and Andriesse, P.A.M., 1983, Laramide and Neogene structure of the Sangre de Cristo Range, south-central Colorado, *in* Lowell, J.D., ed., Rocky Mountain Foreland Basins and Uplifts: Denver, Colorado, Rocky Mountain Association of Geologists, p. 219–228.

Lindsey, D.A., Clark, R.F., and Soulliere, S.J., 1986, Minturn and Sangre de Cristo Formations of southern Colorado: A prograding fan delta and alluvial fan sequence shed from the Ancestral Rocky Mountains, *in* Peterson, J.A., ed., Paleotectonics and Sedimentation: American Association of Petroleum Geologists Memoir 41, p. 541–561.

Lindsey, D.A., Klein, T.L., Valdez, A., and Webster, R.J., 2012, Geology along Mosca Pass Trail, Great Sand Dunes National Park and Preserve, Colorado: U.S. Geological Survey Circular 1374, 18 p.

Madole, R.F., Romig, J.H., Aleinikoff, J.N., VanSistine, D.P., and Yacob, E.Y., 2008, On the origin and age of the Great Sand Dunes, Colorado: Geomorphology, v. 99, p. 99–119, doi:10.1016/j.geomorph.2007.10.006.

Madole, R.F., Mahan, S.A., Romig, J.H., and Havens, J.C., 2013, Constraints on the age of the Great Sand Dunes, Colorado, from subsurface stratigraphy and OSL dates: Quaternary Research, v. 80, p. 435–446, doi:10.1016/j.yqres.2013.09.009.

Nettleton, L.L., 1942, Determination of density for reduction of gravimeter observations: Geophysics, v. 4, p. 176–183, doi:10.1190/1.0403176.

Phillips, J.D., 2001, Designing matched bandpass and azimuthal filters for the separation of potential-field anomalies by source region and source type: Australian Society of Exploration Geophysicists Extended Abstracts, v. 2001, 15th Geophysical Conference and Exhibition, CD-ROM, 4 p., doi:10.1071/ASEG2001ab110.

Popenoe, P., and Steven, T.A., 1969, Interpretation of the aeromagnetic pattern of the San Juan primitive area, Colorado: U.S. Geological Survey Open-File Report 69-211, 7 p.

Ruleman, C., and Machette, M., 2007, An overview of the Sangre de Cristo fault system and new insights to interactions between Quaternary faults in the northern Rio Grande rift, *in* Machette, M.N., Coates, M.M., and Johnson, M.L., eds., 2007 Rocky Mountain Section Friends of the Pleistocene Field Trip: Quaternary Geology of the San Luis Basin of Colorado and New Mexico, September 7–9, 2007: U.S. Geological Survey Open-File Report 2007-1193, p. 187–197.

Ruleman, C.A., Thompson, R.A., Shroba, R.R., Anderson, M., Drenth, B.J., Rotzien, J., and Lyon, J., 2013, Late Miocene–Pleistocene evolution of a Rio Grande rift subbasin, Sunshine Valley–Costilla Plain, San Luis Basin, New Mexico and Colorado, *in* Hudson, M.R., and Grauch, V.J.S., eds., New Perspectives on Rio Grande Rift Basins: From Tectonics to Groundwater: Geological Society of America Special Paper 494, p. 47–73, doi:10.1130/2013.2494(03).

Sales, J.K., 1983, Collapse of Rocky Mountain basement uplifts, *in* Lowell, J.D., ed., Rocky Mountain Foreland Basins and Uplifts: Denver, Colorado, Rocky Mountain Association of Geologists, p. 79–97.

Siebenthal, C.E., 1910, The San Luis Valley, Colorado: Science, v. 31, p. 744–746, doi:10.1126/science.31.802.744-b.

Spiegel, Z., and Baldwin, B., 1963, Geology and water resources of the Santa Fe area, New Mexico: U.S. Geological Survey Water-Supply Paper 1525, 258 p.

Syberg, F.R.J., 1972, A Fourier method for the regional-residual problem of potential fields: Geophysical Prospecting, v. 20, p. 47–75, doi:10.1111/j.1365-2478.1972.tb00619.x.

Thompson, R.A., Shroba, R.R., Machette, M.N., Fridrich, C.J., Brandt, T.R., and Cosca, M.A., 2015, Geologic map of the Alamosa 30′ × 60′ quadrangle, south-central Colorado: U.S. Geological Survey Scientific Investigations Map 3342, 23 p., scale 1:100,000, http://dx.doi.org/10.3133/sim3342.

Tweto, O., 1975, Laramide (Late Cretaceous–early Tertiary) orogeny in the Southern Rocky Mountains, *in* Curtis, B.F., ed., Cenozoic History of the Southern Rocky Mountains: Geological Society of America Memoir 144, p. 1–44, doi:10.1130/MEM144-p1.

Valdez, A., Forman, S., Madole, R., McCalpin, J., Machette, M., Schumann, R., Rupert, M., Mahan, S., and Bunch, F., 2007, Chapter A—Field Trip Day 1: Quaternary geology of Great Sand Dunes National Park and Preserve, southern Colorado, *in* Machette, M.N., Coates, M.M., and Johnson, M.L., eds., 2007 Rocky Mountain Section Friends of the Pleistocene Field Trip: Quaternary Geology of the San Luis Basin of Colorado and New Mexico, September 7–9, 2007: U.S. Geological Survey Open-File Report 2007-1193, p. 3–50.

Wallace, A.R., 2004, Evolution of the southeastern San Luis basin margin and the Culebra embayment, Rio Grande rift, southern Colorado, *in* Brister, B.S., Bauer, P.W., Read, A.S., and Lueth, V.W., eds. , Geology of the Taos Region: New Mexico Geological Society 55th Fall Field Conference Guidebook, p. 181–192.